Transport of Newly Synthesized Sterol to the Sterol-Enriched Plasma Membrane Occurs via Nonvesicular Equilibration†

Nikola A. Baumann,‡,§ David P. Sullivan,‡ Henna Ohvo-Rekilä,‡ Cedric Simonot,‡,|| Anita Pottekat,‡ Zachary Klaassen,⊥ Christopher T. Beh,⊥ and Anant K. Menon*,‡

Department of Biochemistry, University of Wisconsin, 433 Babcock Drive, Madison, Wisconsin 53706, and Department of Molecular Biology and Biochemistry, Simon Fraser University, Burnaby, British Columbia V5A 1S6, Canada

Received August 9, 2004; Revised Manuscript Received February 10, 2005

ABSTRACT: The mechanism by which newly synthesized sterols are transported from their site of synthesis, the endoplasmic reticulum (ER), to the sterol-enriched plasma membrane (PM) is not fully understood. Studies in mammalian cells suggest that newly synthesized cholesterol is transported to the PM in Golgi-bypassing vesicles and/or via a nonvesicular process. Using the yeast *Saccharomyces cerevisiae* as a model system, we now rule out an essential role for known vesicular transport pathways in transporting the major yeast sterol, ergosterol, from its site of synthesis to the PM. We use a cyclodextrin-based sterol capture assay to show that transport of newly synthesized ergosterol to the PM is unaltered in cells defective in Sec18p, a protein required for almost all intracellular vesicular trafficking events; we also show that transport is not blocked in cells that are defective in formation of transport vesicles at the ER or in vesicle fusion with the PM. Our data suggest instead that transport occurs by equilibration ($t_{1/2} \sim 10-15$ min) of ER and PM ergosterol pools via a bidirectional, nonvesicular process that is saturated in wild-type exponentially growing yeast. To reconcile an equilibration process with the high ergosterol concentration of the PM relative to ER, we note that a large fraction of PM ergosterol is found condensed with sphingolipids in membrane rafts that coexist with free sterol. We propose that the concentration of free sterol is similar in the PM and ER and that only free (nonraft) sterol molecules have access to a nonvesicular transport pathway that connects the two organelles. This is the first description of biosynthetic sterol transport in yeast.

Sterols are unevenly distributed in the endomembrane system of eukaryotic cells (*1*−*7*). They exist in the plasma membrane (PM)[1] at high concentrations, where they restrict the flexibility of phospholipid acyl chains, thicken the PM (*3*, *6*), and decrease its permeability to small molecules (*3*, *7*). Sterol concentration in the ER is low, consistent with the need for a more fluid membrane to accommodate processes such as membrane protein translocation (*8*). In the PM and to a certain extent in the ER, sterols are found in condensed complexes with sphingolipids and other phospholipids with saturated fatty acyl chains (*9*−*13*). These complexes form the lipid underpinning of rafts, membrane domains that are hypothesized to serve as platforms for signal transduction or cargo sorting in exocytic and endocytic traffic (*14*). The sterol−sphingolipid complexes may be envisaged to constitute a liquid ordered (l_o) phase where lipid acyl chains are fully extended and tightly packed, surrounded by a sea of liquid disordered (l_d) lipids (*10*−*13*). The l_o and l_d states can be biochemically separated by extracting membranes in cold nonionic detergents to yield detergent-insoluble membranes (DIMs)[2] corresponding to l_o lipids and their associated proteins and detergent-soluble material corresponding to l_d lipids and associated proteins (*10*−*13*). Unlike free sterols, sterols in condensed complexes have a reduced off rate from membranes and a diminished ability to participate in collisional transfer events between membrane compartments or between membranes and soluble acceptors (*11*, *15*−*17*).

Previous analyses in mammalian cells showed that newly synthesized cholesterol is transported from the ER to the PM via an ATP-dependent, brefeldin A (BFA)-insensitive process

† This work was supported by grants from the National Institutes of Health (GM55427), American Heart Association (Northland Affiliate Grant 0051598Z), the Hatch−McIntire−Stennis program (project 3855) (all to A.K.M.), and by a Natural Sciences and Engineering Research Council of Canada (NSERC) grant (to C.T.B.). N.A.B. and A.P. were supported by fellowships from the Department of Biochemistry. H.O.-R. was supported by a fellowship from the Academy of Finland and by grants from the Magnus Ehrnrooth Foundation and Medicinska Understödföreningen Liv och Hälsa.

* To whom correspondence should be addressed: Department of Biochemistry, University of Wisconsin−Madison, 433 Babcock Drive, Madison, WI 53706-1569. Telephone: +1-608-262-2913. Fax: +1-608-262-3453. E-mail: menon@biochem.wisc.edu.

‡ University of Wisconsin.

§ Present address: Washington University School of Medicine, 660 S. Euclid Ave., St. Louis, MO 63110.

|| Present address: Fondation Gillet-Merieux, bat 3B, Lyon-Sud Hospital, 69495 Pierre-Benite, France.

⊥ Simon Fraser University.

[1] Abbreviations: BFA, brefeldin A; DIM, detergent-insoluble membrane; ER, endoplasmic reticulum; lcb, long-chain base; LRV, lipid-rich vesicle; MβCD, methyl-β-cyclodextrin; PL, phospholipid; PM, plasma membrane; RP-HPLC, reversed-phase HPLC; RSR, relative specific radioactivity; SR, specific radioactivity.

[2] In this paper, we use the operationally defined term DIM synonymously with the terms "raft" and "sterol−sphingolipid-condensed complex".

10.1021/bi048296z CCC: $30.25 © 2005 American Chemical Society
Published on Web 03/19/2005

that is disrupted at 15 °C (*18*−*21*). The 15 °C temperature block caused newly synthesized cholesterol to accumulate in the ER as well as in low density, lipid-rich vesicles (LRV) (*19*, *20*). On the basis of the evidence of a BFA-resistant yet temperature-sensitive sterol transport pathway involving a LRV intermediate, Simoni and co-workers suggested that there must exist a Golgi-bypassing vesicular route available to sterols but inaccessible to cell-surface proteins (*20*). More recent data indicate that BFA does block part of the sterol flux to the PM and that a small fraction of newly synthesized sterols is routed through the Golgi, acquiring DIM characteristics en route to the PM (*21*). On the basis of these results, it would appear that newly synthesized sterols are transported to the PM via a largely BFA-resistant vesicular transport pathway or via a nonvesicular mechanism. Using yeast as a model system (*22*), we now rule out an essential role for known vesicular transport pathways in transporting ergosterol, the major yeast sterol. Our data indicate that transport occurs by equilibration ($t_{1/2} \sim 10$ min) of ER and PM ergosterol pools via a bidirectional, nonvesicular process that is saturated under exponential growth conditions. To reconcile the equilibration of ER and PM sterol pools with the ~10-fold enrichment of ergosterol in the PM relative to ER, we note that a large fraction of PM sterol is found condensed with sphingolipids in membrane rafts that coexist with free sterol. We propose that the concentration of free sterol is similar in the PM and ER and that it is the free (nonraft) sterol pool that has access to a nonvesicular transport pathway that connects the two organelles and possibly also other internal membranes.

EXPERIMENTAL PROCEDURES

Materials. [^{3}H-methyl]Methionine (80 Ci/mmol) and *myo*-[2-^{3}H]inositol (60 Ci/mmol) were purchased from American Radiolabeled Chemicals (St. Louis, MO). Methyl-β-cyclodextrin (MβCD), cholesterol, ergosterol, lathosterol, lanosterol, squalene, 7-dehydrocholesterol, desmosterol, filipin, and silver nitrate were from Sigma (St. Louis, MO). Propidium iodide was purchased from Molecular Probes (Eugene, OR) and RenoCal-76 from Bracco Diagnostics (Princeton, NJ). Solvents were HPLC-grade and purchased from Fisher Scientific (Fair Lawn, NJ). Silica 60 thin-layer chromatography plates were from Merck (Darmstadt, Germany). Yeast extract, yeast nitrogen base, bacto peptone, and dextrose were from Difco Laboratories (Detroit, MI).

Yeast Strains and Growth Conditions. Yeast cultures were grown in YPD (1% yeast extract, 2% bacto peptone, and 2% dextrose) or synthetic complete medium without methionine (SC-met) (6.7 g/L yeast nitrogen base without amino acids and 20 g/L dextrose, supplemented with amino acids but lacking methionine). Ergosterol transport assays were performed on mid-log phase cultures ($OD_{600} \sim 5.0$) started from 0.5 to 1 mL of stationary phase culture in 50 mL of YPD and grown overnight at room temperature. All stationary phase cultures of secretory mutants were tested for temperature-sensitive growth before experiments were performed.

Temperature-sensitive yeast secretory mutants used in this study were RSY255 (wild type; MATα *ura3*−*52 leu2*−*3112*), RSY 782 (MATα *sec1*−*1 ura3*−*52 his4*−*619*), RSY263 (*sec12*−*4 ura3*−*52 leu2*−*3,112*), and RSY271 (*sec18*−*1 ura3*−*52 his4*−*619*) (provided by Dr. Charles K. Barlowe, Dartmouth Medical School, Hanover, NH) (*23*, *24*). Wild-type strain RH1800 (MATα *leu2 his4 ura3 bar1*) and the *lcb1*−*100* mutant RH3809 (MATα *his4 end8 ura3 leu2 bar1 lcb1*−*100*) were from Dr. Howard Riezman (Biozentrum of the University of Basel, Switzerland) (*25*).

Metabolic Labeling of Ergosterol and Methyl-β-cyclodextrin (MβCD) Capture Assay. Overnight cultures (50 mL at $OD_{600} \sim 5.0$) were collected by centrifugation (3000*g* at 10 min) and washed once with water. For experiments using temperature-sensitive yeast *sec* mutants or *lcb1*−*100* mutants, cells were resuspended in 4 mL of SC-met and incubated in an orbital-shaking water bath at 37 °C (restrictive temperature) for 25 or 5 min, respectively, to induce the mutant phenotype before metabolic labeling. The parent wild-type strains were treated identically. [^{3}H-methyl]Methionine (0.8−1 mCi in 250 μL of labeling medium) was then added, and cells were pulse-labeled for 4 min at 37 °C. After labeling, 16 mL of chase medium [16 mL of SC-met containing 25% methionine solution (20 mg/mL final concentration)] were added and cells were incubated in a shaking water bath at 37 °C for the duration of the chase period.

To test the effect of energy poisons on transport, 10 mM NaF and 10 mM NaN_3 were included in the chase media; to test the effect of low temperature, ice-cold chase medium was added to the cell suspension immediately following the pulse-labeling period and the cells were incubated on ice with frequent shaking.

At indicated times, cells were taken for ergosterol efflux assays. A total of 1 mL of cells was transferred to a 2 mL microfuge tube on ice. MβCD was then added from a 0.25 M stock solution in water (40 mM final concentration), and cells were incubated on ice for 20 min. After incubation, the cells were centrifuged for 1 min (13000*g* at 0 °C) and the MβCD-containing supernatant was removed and centrifuged again to remove any remaining cells. The cell pellet was resuspended in 1 mL of water, and lipid extraction of both the supernatant and cells was performed. Aliquots of cells taken after MβCD extraction were tested for viability by measuring their ability to exclude propidium iodide according to Deere et al. (*26*). A total of 1 mL of mock-treated cells was processed in parallel to determine the extent of spontaneous efflux of ergosterol into the medium.

Lipids in the MβCD extract and in the cell pellet were analyzed by RP-HPLC as described under "lipid extraction and analysis", and the specific radioactivity (SR) of ergosterol [cpm/AU, counts per minute (cpm) of [^{3}H]ergosterol/absorbance units (AU) at 280 nm (total ergosterol)] was determined. The SR for the cell samples rapidly reached a plateau value indicating effective chase conditions. This plateau value (obtained by curve fitting to a monoexponential function (see Figure 2A, for example) or by averaging all SR values for time points >10 min) was used to normalize the SR values for ergosterol in the MβCD extract, yielding a relative specific radioactivity (RSR). Thus, RSR (MβCD extract) = SR (MβCD extract)/SR plateau (cells). RSR directly compares the specific radioactivity of PM-localized ergosterol extracted by MβCD with that of total cellular ergosterol. The RSR calculation also provides a simple way of consolidating data from different experiments where the extent of metabolic labeling can vary.

Lipid Extraction and Analysis for the MβCD Capture Assay. Lipids were extracted from cells or MβCD-containing supernatant using the Folch method. Briefly, a 1 mL aqueous sample was added to 5 mL of chloroform/methanol (2:1, v/v) in a glass tube and vortexed. The organic phase was washed with mock upper phase before being dried in a SpeedVac evaporator and redissolved in 1 mL of chloroform/methanol (1:1, v/v). Aliquots were taken for liquid scintillation counting and reverse-phase-high-pressure liquid chromatography (RP-HPLC) analyses. Samples to be analyzed by RP-HPLC were filtered through a 0.2 μm syringe filter before injection.

RP-HPLC analyses of lipid extracts were conducted on a C18 spherisorb column (S5 ODS2, 4.6 × 250 mm) (Waters, Milford, MA) (*27*). Sterols were manually injected using a 200 μL injection loop, eluted with methanol/water (95:5, 1 mL/min), detected at 280 nm using a Waters 2487 detector and quantified using a Waters 746 data module integrator. Detector response to sterol was calibrated, and measurements were carried out in a linear response range. Elution fractions (0.7 mL) were collected, and radioactive sterol was quantified by scintillation counting. Data obtained from RP-HPLC and scintillation counting were expressed as SR (cpm/AU).

Isolation of DIMs. Aliquots (1.8 mL) of cells were taken during a pulse-chase experiment (as above) at indicated times after the beginning of the chase. Cells were collected by centrifugation (2500*g* for 5 min at 4 °C), resuspended in 500 μL of TEPI [100 mM Tris-HCl at pH 7.5 and 10 mM EDTA, with 1× Protease Inhibitor Cocktail (Calbiochem)] and lysed by vortexing with 0.5 volume of glass beads for 6 cycles (30 s vortexing and then 30 s incubation on ice.) Unbroken cells were removed by centrifugation (2500*g* for 5 min at 4 °C). The supernatant was collected and replaced with fresh TEPI (500 μL), which was then vortexed once for 30 s and centrifuged again as before. The combined supernatants were centrifuged again (2500*g* for 5 min at 4 °C) to remove any remaining unbroken cells and debris. A total of 500 μL of the cleared supernatant was combined with an equal volume of TEPI plus 2% Triton X-100, to give a final concentration of 1% Triton X-100, and incubated on ice for 30 min. DIMs were collected by centrifugation for 30 min at 4 °C in a TLA 100.3 rotor at 60 000 rpm (∼200000*g*). The supernatant was removed for lipid extraction by the Folch method as described above, while the pellet was resuspended in 1 mL of TEPI plus 1% Triton X-100 and then extracted.

Analysis of Sterol and Sterol Ester Levels in Whole Cells. Cells were disrupted by vortexing with glass beads before extracting lipids with 3 mL of hexane/2-propanol (3:2, v/v) per 1 mL of aqueous phase. 7-Dehydrocholesterol was added to each extract as an internal standard for RP-HPLC analysis [20 nmol for cellular extracts and 3 nmol for RenoCal-76 fractions (see below)]. The organic phase was collected, and the aqueous phase was re-extracted with 3 mL of hexane. The combined phase was washed with 1 mL of water and then evaporated to dryness. The sterols were dissolved in methanol and separated on RP-HPLC as previously described. The amount of ergosterol in each fraction was calculated from the chromatogram peak area compared to a series of ergosterol standards with known concentrations. Possible deviations between different RP-HPLC runs were corrected by normalizing to the peak area of the 7-dehydrocholesterol internal standard. Sterol esters were determined by RP-HPLC quantitation of sterols in samples before and after saponification. For saponification, the total cellular lipid extract was evaporated, saturated ethanolic NaOH was added, and the samples were heated at 95 °C for 2 h. Sterols were extracted twice with hexane. The increase in the sterol amount obtained after saponification was taken as the amount of sterol ester (the internal standard, 7-dehydrocholesterol, was used to control for losses).

In initial experiments, HPLC-purified sterols were characterized by gas chromatography−mass spectroscopy (GC−MS), UV spectroscopy, and silver nitrate TLC to establish their identity. GC−MS analyses were conducted on a Finnigan MAT (San Jose, CA) ion-trap mass spectrometer (Magnum) in EI mode (manifold temperature at 220 °C, filament at 10 μA, electron multiplier at 1700 V, and scanning range of 45−450 amu at 1 s/scan). The ion trap was coupled to a Varian Gas Chromatograph equipped with split/splitless injector. A Restek RTX-5MS fused silica capillary column (30 ms, 0.25 mm inside diameter, 0.25 μm film thickness) was interfaced directly to the ion trap. UV spectra of RP-HPLC purified sterols were recorded in methanol/water (95:5, v/v) between 190 and 350 nm on a Shimadzu UV-1601 spectrometer.

RenoCal Gradient Analysis of PM Fractions from Wild-Type and lcb1−100 Cells. Total cellular membranes from ∼20 OD_{600} units of cells (grown to OD_{600} ∼ 1 at room temperature and then incubated for 1 h at 37 °C as indicated) were fractionated on RenoCal-76 gradients exactly as described (*28*, *29*). Wild-type (RH1800) and *lcb1−100* (RH3809) cells were fractionated in parallel. A total of 14 0.35-mL fractions were collected from the top of each gradient. Membranes in a 50-μL aliquot of each fraction were diluted with water, pelleted by ultracentrifugation, and taken for SDS−PAGE and immunoblotting analysis with antibodies against Gas1p and Pma1p (PM markers), Sec61p (ER), Pep12p (endosomes), and Vph1p (vacuole). As described previously (*28*, *29*), the majority of the Gas1p and Pma1p signal was recovered consistently in fractions 9−11, while the other organellar markers were spread through fractions 1−9.

The PM mass recovered in RenoCal fractions 9−11 was quantitated by densitometric analysis of Gas1p and Pma1p immunoblots. Immunoblots corresponding to RenoCal separations of wild-type and *lcb1−100* membranes were exposed side-by-side on the same film. Multiple exposures were taken to generate blot signals with a range of intensities. The signals were quantitated by densitometry; only signal intensities that were determined to lie within an empirically determined linear response range were used for analysis.

To assess relative PM sterol concentration between *lcb1−100* and wild-type cells, fractions 9−11 of the RenoCal separations of the respective strains were extracted with hexane/2-propanol (3:2, v/v) and hexane as described above and ergosterol content was quantitated by RP-HPLC using 7-dehydrocholesterol as an internal standard. The ratio of ergosterol recovered in fractions 9−11 of the RenoCal separations of *lcb1−100* and wild-type membranes was normalized to the ratio of the corresponding Gas1p (or Pma1p) signal intensity determined from quantitative immunoblotting, to give a relative sterol concentration (sterol/

Gas1p) for *lcb1−100* PM compared with that of wild-type PM set at 1.

Filipin Staining and Fluorescence Microscopy. To examine cellular sterol distribution, yeast cells were fixed and treated with filipin complex as previously described (*30*). After incubation at 37 °C for specific times, cell samples were fixed and stained with 0.1 mg mL^{-1} filipin complex and gently resuspended in residual water. Filipin-stained cells were transferred to polylysine-coated slides, sealed under coverslips with nail polish, and observed with a Orca-ER CCD digital camera (Hamamatsu Photonics, Hamamatsu-City, Japan) mounted on a Leica DMRA2 microscope (Leica Microsystems, Wetzlar, Germany), using a UV filter set and neutral density filters. Images were analyzed using Improvision Open Lab software (Lexington, MA), and cell counting was performed blind on randomized images.

RESULTS AND DISCUSSION

We developed sensitive methods to study the transport of *de novo* synthesized ergosterol from the ER to the PM in yeast, a model system in which vesicular pathways can be abrogated at specific steps using *sec* mutants (*23*, *24*) and sterol trafficking analyses are simplified by the absence of a sterol uptake pathway such as found in mammalian cells (*22*). Yeast synthesize the C28 sterol, ergosterol, instead of cholesterol (Figure 1A). Ergosterol concentration in the yeast PM is 5−10-fold higher than it is in the ER (*5*, *6*; C. S. and A. K. M., unpublished data), similar to the ER/PM cholesterol concentration ratio in mammalian cells (*3*). Ergosterol differs importantly from cholesterol in that it has a methyl group appended to carbon 24 and two additional double bonds that contribute to its greater propensity for forming condensed complexes with sphingolipids (*11*, *31*). RP-HPLC analysis of a Folch lipid extract of yeast yields a simple profile (monitored by absorbance at 280 nm) consisting of a major peak of ergosterol and a minor peak of 22-dihydroergosterol, an ergosterol precursor (Figure 1B). A pulse of radiolabeled [^{3}H]ergosterol can be generated by incubating yeast with [^{3}H-methyl]methionine. Because the methylation reaction occurs late in ergosterol biosynthesis (Figure 1A), it is considerably easier to obtain an effective chase after a labeling pulse with [^{3}H]methionine than with [^{3}H]acetate, a commonly used sterol precursor (*18*−*21*). Pulse-radiolabeling of yeast, lipid extraction, and RP-HPLC analysis yielded a radioactivity profile containing ergosterol, 22-dihydroergosterol, and an uncharacterized biosynthetic intermediate; both intermediates were consumed during the chase (Figure 1C).

ER−PM Sterol Transport Assay. To assay transport of pulse-labeled [^{3}H]ergosterol to the PM, we used methyl-β-cyclodextrin (MβCD), a soluble cyclic oligosaccharide that when added to intact yeast cells is able to extract ergosterol molecules from the outer leaflet of the PM. Cyclodextrin-mediated sterol efflux has been proposed to occur by an activation−collision mechanism in which the partial projection of sterol molecules out of the bilayer precedes collisional capture by cyclodextrin (*15*, *16*, *32*, *33*). Aliquots of metabolically pulse-chase radiolabeled yeast cells were incubated with MβCD on ice and then centrifuged to generate a cell pellet and an MβCD-containing supernatant. The cell pellet and supernatant were separately subjected to lipid extraction and RP-HPLC analysis. To adjust for variations in extraction efficiency, radioactivity (cpm) in RP-HPLC-resolved [^{3}H]ergosterol was normalized to bulk, unlabeled ergosterol in the extract (detected by absorbance (AU) in the same chromatogram; measurements were in a range where absorbance was directly proportional to the amount of ergosterol) to yield a SR (cpm/AU). Under the conditions used, MβCD extracted ∼0.3−0.4% of total cellular ergosterol (no ergosterol was detected in the medium in the absence of MβCD).[3]

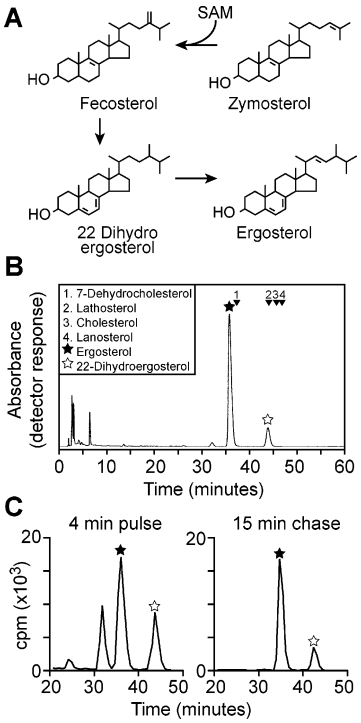

FIGURE 1: Metabolic labeling of ergosterol. (A) Abbreviated biosynthetic scheme showing late steps in the biosynthesis of ergosterol, including the step at which a methyl group from *S*-adenosylmethionine (SAM) is transferred to zymosterol. (B) RP-HPLC analysis of a Folch lipid extract from yeast. The absorbance profile shows a prominent peak of ergosterol (★) and a later-eluting peak (☆) corresponding to the biosynthetic intermediate 22-dihydroergosterol. The identity of the sterols was confirmed by gas chromatography−mass spectroscopy (GC−MS), UV spectroscopy, and silver nitrate thin-layer chromatography. (C) RP-HPLC analyses of lipid extracts from cells taken after a 4 min labeling pulse with [^{3}H-methyl]methionine and after a 15 min chase. The distribution of radioactivity is shown, as are the migration positions of ergosterol (★) and 22-dihydroergosterol (☆). The radioactivity profile at the end of the pulse shows a peak of [^{3}H]ergosterol flanked by peaks corresponding to radiolabeled biosynthetic intermediates. The radioactivity profile at the end of the 15 min chase resembles the absorbance profile shown in B.

Figure 2A shows that the SR of ergosterol in the cell sample rapidly reached a plateau upon initiation of chase conditions.[4] The SR of the MβCD-extracted ergosterol approached a maximum value with a half-time of ∼15 min (Figure 2B), indicating that newly synthesized sterol reaches the PM MβCD-extractable pool rapidly in a time frame of minutes. When the SR data for the MβCD extract were replotted after normalization to the plateau SR value obtained for the cell extract, the transport curve shown in Figure 2C was obtained. A single-exponential fit of these normalized transport data yielded a plateau of ∼1 with $t_{1/2}$ ∼ 15 min. The plateau value of ∼1 is consistent with equilibration of

[^{3}H]ergosterol between the bulk cellular pool and the MβCD-accessible pool.

Transport of radiolabeled sterol to the MβCD-extractable pool was blocked if the cells were chased on ice or in the presence of energy poisons (Figure 2C, □), consistent with data reported previously for cholesterol transport in mammalian cells (*19*−*21*).

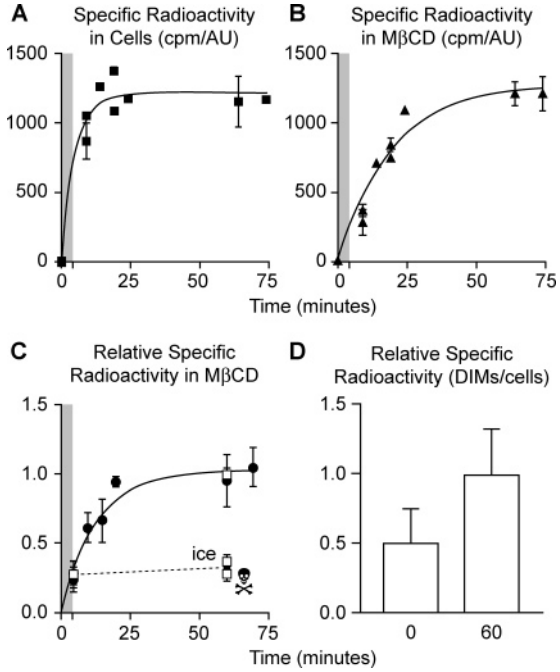

FIGURE 2: Assay of ergosterol transport to the cell surface. Transport of newly synthesized ergosterol to the PM assayed by MβCD extraction. Yeast were pulsed with [^{3}H-methyl]methionine for 4 min (indicated by the gray bar in each panel) and then chased with unlabeled methionine. Cells were withdrawn at the indicated time points and incubated with MβCD on ice. Cell pellets and MβCD extracts were subjected to lipid extraction and RP-HPLC analysis. (A) Specific radioactivity [cpm per absorbance units (AU)] of ergosterol in the cell sample. (B) Specific radioactivity of ergosterol in the MβCD extract. (C) Relative specific radioactivity of ergosterol (●) during the pulse-chase time course obtained by normalizing the specific radioactivity of ergosterol in the MβCD extract to the SR plateau of the cell sample. Cells were shown to remain intact throughout the MβCD extraction procedure by demonstrating their ability to exclude propidium iodide. The figure also shows that transport is blocked when cells are incubated on ice or treated with energy poisons during the chase period (□): cells were pulse-labeled, and aliquots were left on ice, treated with energy poisons, or left untreated (control) before being processed by MβCD extraction at the 60 min time point. (D) Recovery of unlabeled (cold) ergosterol and [^{3}H]ergosterol in DIMs. Samples taken at the end of a 4 min [^{3}H-methyl]methionine-labeling pulse (chase = 0 min) and after a 60 min chase were placed on ice and treated with Triton X-100 (see the Experimental Procedures) to determine the fraction of total labeled and unlabeled ergosterol in DIMs.

Newly Synthesized Ergosterol in DIMs. The proportion of newly synthesized sterol that was raft-associated during ER−PM transport was gauged by measuring the percent [^{3}H]-ergosterol that could be recovered in DIMs at the end of the pulse versus the end of the chase. Recovery of bulk, unlabeled ergosterol in DIMs was ∼70% of the total at both time points consistent with a previous report (*37*), whereas newly synthesized [^{3}H]ergosterol was largely detergent-soluble at the end of the pulse but participated in DIMs to the same extent as unlabeled ergosterol at the end of the chase (Figure 2D). Thus, the relative specific radioactivity of ergosterol in DIMs (versus total cellular ergosterol) was ∼0.49 at the end of the pulse and ∼1 at the end of the chase (Figure 2D). These data indicate that [^{3}H]ergosterol is initially more detergent-soluble but equilibrates with the DIM-associated bulk sterol after 60 min. The value of ∼0.49 for the relative specific activity of ergosterol in DIMs at the end of the pulse period is likely a result of transport of a

[3] Longer incubations with MβCD or incubations of cells with MβCD at room-temperature rather than on ice did not improve sterol extraction yield much beyond the ∼0.3% value obtained under standard conditions. Also, spheroplasting had no significant effect on ergosterol extractability. While we have yet to understand fully why extraction efficiency is so low, we offer some discussion of this issue in this footnote. We also note that the low extraction efficiency is an advantage because it reduces the chance that intracellular sterol pools are mobilized or that cell viability is compromised. We assume that MβCD extracts ergosterol principally from the free ergosterol pool in the PM because of (a) the known propensity of free versus complexed sterol for extraction by a collision-based process (*11*, *15*−*17*) and (b) the higher extraction efficiency (∼3%) seen with the sphingolipid-poor *lcb1*−*100* mutant (Table 1), where the cellular (and hence PM) amounts of free ergosterol are higher [this correlates with the lower recovery of sterols in DIMs in *lcb1*−*100* versus wild-type cells (Table 1)]. The simplified sterol distribution/transport model that we propose in Figure 4 suggests that the majority of ergosterol in yeast is located in the PM in the form of condensed complexes and that only ∼8% of the total cellular ergosterol is extractable by MβCD (corresponding to the fraction of total cellular sterol that exists as free sterol in the PM) assuming no sterol movement between pools under extraction conditions. If there exist pools of ergosterol in intracellular membranes other than the ER [these pools would have to be relatively small in wild-type cells where most sterol is located in the PM as seen by filipin staining (panel 1 of Figure 5B and ref *30*) as well as by RenoCal gradient separation of PM from total microsomes (ref *29* and unpublished data)], the percent of MβCD-extractable ergosterol would be lower than 8%. However, it is unlikely to be as low as the experimentally observed level of <1%, suggesting that the explanation for the low extraction efficiency lies elsewhere. We considered the possibility that there are two pools of free ergosterol in the PM, one of which is inaccessible to MβCD. Our data indicate that, even if there are two pools of free ergosterol in the PM, they are ultimately metabolically indistinguishable from each other and from complexed ergosterol because all pools achieve the same SR by the end of the chase period. Is it possible to have metabolically indistinguishable yet MβCD-resistant and accessible pools of free ergosterol at the PM? Transverse segregation of pools in opposite leaflets of the PM bilayer or lateral segregation of ergosterol pools into different PM regions (bud versus cell body, for example) may provide ways to generate MβCD-resistant and accessible populations. We discount these particular possibilities because sterol flip-flop is rapid under our low-temperature extraction conditions (*32*, *34*) and spheroplasting (which would be reasonably expected to eliminate macroscopic PM regionalization) has little effect on extraction efficiency. We are left with the interesting idea (suggested to us by F. R. Maxfield at Cornell University) that extraction of a very small fraction of PM sterol may result in "freezing" the PM lipid milieu, blocking further extraction. In support of this idea are data demonstrating that lateral diffusion of lipid probes and proteins in the yeast PM is unusually low (even in spheroplasts) and that the PM may have a semifrozen physical character that is exacerbated by removing a small fraction of its sterol content (*35*, *36*). This is a potentially testable idea that will be pursued in future work. For the purposes of this paper, the MβCD extract appears to provide a credible and reproducible way to monitor the arrival of a pulse of newly synthesized ergosterol at the PM.

[4] A fraction of the total sterol in yeast is in the form of steryl esters that are presumably exclusively located in lipid droplets (*22*). Under our assay conditions (37 °C), ergosterol ester represented 15 ± 1% (mean ± SEM) of the total ergosterol in RH1800 cells and the level of ester remained constant during the chase period (the proportion of ergosterol in the form of ester was 13 ± 3% for logarithmically growing cells maintained at 23 °C). Incorporation of radioactivity into the ester pool was rapid, with the SR of the ergosterol ester pool remaining essentially constant throughout the chase (data not shown). This is consistent with equilibration of ergosterol esters with total ergosterol. See Table 1 for detailed results.

fraction of the labeled ergosterol to the PM by this time point (Figure 2C) and also some complex formation between [^{3}H]-ergosterol and sphingolipid precursors in the ER as described previously (*37*). These data complement our MβCD assay results and suggest that newly synthesized sterol equilibrates with both detergent-insoluble and MβCD-accessible PM pools of sterol over a similar time frame.

ER−PM Ergosterol Transport Does Not Require the Secretory Pathway. The classical secretory pathway is required for the transport of proteins and complex sphingolipids from the ER/Golgi to the PM in yeast. Protein or lipid cargo is sorted into vesicles that bud from a donor compartment such as the ER; these vesicles then dock and fuse with their target membrane, thus effecting cargo delivery. Sec18p, the yeast homologue of mammalian NSF (*38*, *39*), is involved in vesicle fusion. Upon shifting to restrictive temperature, the temperature-sensitive *sec18−1* yeast mutant exhibits a rapid block at most intercompartmental transport steps in the secretory pathway, with the exception of post-Golgi−vacuole transport (*39*), and accumulates 50-nm diameter vesicles in the cytoplasm. To determine whether a functional defect in Sec18p affects ER−PM sterol transport, *sec18−1* cells were grown overnight at the permissive temperature (24 °C), then transferred to labeling medium, and shifted to the restrictive temperature (37 °C) for 25 min before pulse-chase labeling with [^{3}H-methyl]methionine. Pulse-chase labeling and MβCD efflux assays were performed as described above followed by lipid extraction and RP-HPLC analyses of the lipid extracts.

Figure 3C (derived from the raw data shown in parts A and B of Figure 3) shows that *sec18−1* cells display rapid ER−PM ergosterol transport at the nonpermissive temperature ($t_{1/2} \sim 15$ min), indistinguishable from that seen in a parallel assay with an isogenic wild-type strain. Because vesicular transport between the ER, Golgi, and PM requires Sec18p, these results suggest that the secretory pathway is not required for transport of newly synthesized ergosterol to the PM.

Although it has been reported that the secretion block is induced less than 1 min after shifting *sec18−1* cells to restrictive temperature (*39*), we wanted to verify that the *sec18−1* phenotype was induced under our labeling conditions. We first confirmed that secretion of metabolically radiolabeled proteins into the medium was abrogated in *sec18−1* cells at 37 °C (not shown) and then tested the effect of the *sec18−1* block on a lipid transport pathway known to require vesicular transport. In yeast, the synthesis of complex sphingolipids, such as IPC, occurs in the Golgi (*40*) and requires transport of ceramide from the ER to the Golgi by both vesicular and nonvesicular transport mechanisms (*41*). It has been previously shown that IPC synthesis is greatly reduced in *sec* mutants with defects in ER to Golgi transport and that under these conditions synthesis of downstream sphingolipids (MIPC and M(IP)$_2$C) from [^{3}H]-inositol is virtually undetectable (*41*, *42*). We labeled *sec18−1* and wild-type cells with [^{3}H]inositol at 37 °C and measured synthesis of radiolabeled IPC, MIPC, and M(IP)$_2$C as described by Puoti et al. (*42*). Synthesis of [^{3}H]sphingolipids (normalized to [^{3}H]PI synthesis, which is independent of the secretory pathway) was reduced by 87% in *sec18−1* cells at 37 °C compared to that in wild-type cells, confirming that the secretion block was effective under our labeling conditions. These results establish that, while protein secretion is blocked and secretory pathway-dependent lipid metabolism is reduced ~10-fold in *sec18−1* cells at 37 °C, transport of newly synthesized ergosterol from the ER to the PM is unaffected.

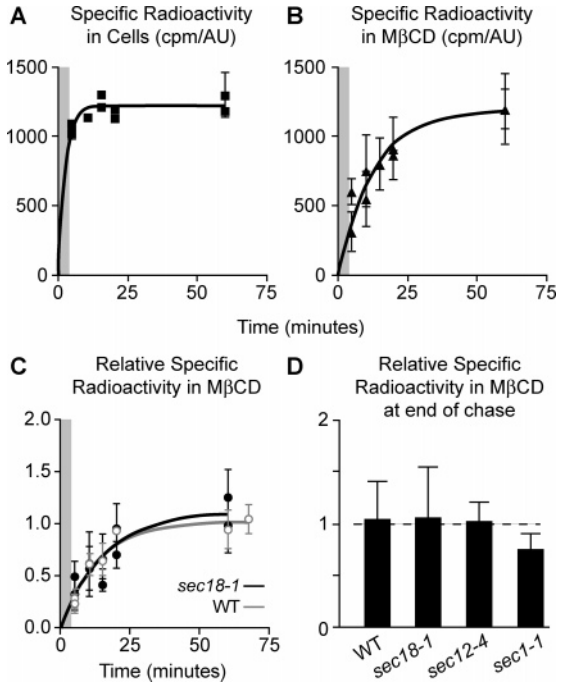

FIGURE 3: Abrogation of vesicular transport does not block delivery of newly synthesized ergosterol to the PM. (A−C) Secretion-defective *sec18−1* cells were incubated at 37 °C for 25 min to induce the mutant phenotype before pulse-chase metabolic labeling with [^{3}H-methyl]methionine. The pulse period is indicated by the gray bar in each panel. Cells were withdrawn at the indicated time points and incubated with MβCD on ice. Cell pellets and MβCD extracts were subjected to lipid extraction and HPLC analysis. The panel at the left shows the specific radioactivity of ergosterol in the cell sample, the middle panel shows the specific radioactivity of ergosterol in the MβCD extract, and the right panel represents the relative specific radioactivity of ergosterol during the pulse-chase time course obtained by normalizing the specific radioactivity of ergosterol in the MβCD extract to the SR plateau of the cell sample (black data points and line). Data from two transport experiments are shown. An isogenic wild-type strain was processed identically to yield the data points (○) and transport curve in gray in the right panel. (D) Summary of data for transport of newly synthesized ergosterol to the PM in the wild-type, *sec18−1*, *sec12−4*, and *sec1−1* strains at 37 °C. Data represent the average of at least two experiments. The bar chart shows the relative specific radioactivity of ergosterol in the MβCD extract at the end of the chase period (60 min) (data are taken from C for wild-type and *sec18−1* cells; representative data for *sec12−4* are SR (MβCD) and SR (cell) = 432 ± 42 and 453 ± 40 cpm/AU, respectively; representative data for *sec1−1* are SR (MβCD) and SR (cell) = 545 ± 8 and 604 ± 40 cpm/AU, respectively). With the exception of *sec1−1*, newly synthesized ergosterol equilibrates within 60 min in all strains to yield a relative specific radioactivity in the MβCD extract of ~1 (indicated by a line corresponding to an ordinate value of 1). For *sec1−1*, equilibration is reached somewhat more slowly with an average relative specific radioactivity in the MβCD extract of ~0.75 at 60 min.

Transport of newly synthesized ergosterol is not blocked in mutants with defects in early and late steps of the secretory pathway. Experiments with the *sec18−1* mutant demonstrated that inhibiting the secretory pathway had no effect on ergosterol transport to the PM. Although Sec18p is required for all vesicle fusion events between the ER and

PM (*39*), we wanted to confirm these results by assaying transport in mutants with defects in vesicle budding from the ER (*sec12−4*) and in Golgi to PM transport (*sec1−1*). Sec12p is the guanine nucleotide exchange factor of Sar1p and is required for recruitment of the COPII coat onto ER membranes (*43*), while Sec1p is needed for fusion of Golgi-derived transport vesicles with the PM (*44*).

Temperature-sensitive *sec12−4* and *sec1−1* mutant strains were incubated at 37 °C (the restrictive temperature) for 25 min before pulse-chase labeling with [^{3}H-methyl]methionine. *Sec12−4* cells were also radiolabeled with [^{3}H]inositol to examine vesicular transport-dependent sphingolipid synthesis: [^{3}H]sphingolipid synthesis was reduced >80% compared to that in wild-type cells, verifying that vesicular transport from the ER to Golgi apparatus was blocked. Unlike the transport of sphingolipids and proteins, transport of newly synthesized [^{3}H]ergosterol to a MβCD-extractable PM pool was not blocked in the *sec12−4* and *sec1−1* strains at 37 °C (compared in each case to the isogenic wild-type strain) (Figure 3D). However, transport was modulated in these mutants such that the transport curve displayed a short lag in one case (*sec12−4*) or a longer half-time (*sec1−1*) (data not shown). These results were unexpected because the kinetics of transport in *sec18−1* mutants were identical to that in wild type cells, suggesting that a functional secretory pathway is not required for the ER−PM ergosterol transport. Furthermore, Sec18p is required downstream of Sec12p in the ER−Golgi transport and downstream of Sec1p for the fusion of secretory vesicles with the PM. Protein secretion is known to be completely blocked in all of these *sec* mutants, while [^{3}H]ergosterol transport was either unaffected or slow but not blocked. When these results are taken together, they suggest that the lag in transport and slower kinetics observed in *sec12−4* and *sec1−1* strains, respectively, are due to complex indirect effects of the mutant phenotypes (such as expansion of the total ER membrane area in *sec12−4* and proliferation of vesicles in the vicinity of the PM in *sec1−1*) rather than a direct effect of the loss of a component of the vesicular transport pathway.

We conclude that the classical secretory pathway is not required to deliver newly synthesized ergosterol from the ER to the PM and that yeast cells possess a high capacity vesicle-independent sterol transport pathway that compensates entirely for the loss of vesicular traffic in *sec* mutants. We note that our data do not rule out the possibility that sterols may be transported in secretory vesicles or that sterols may be sorted or involved in sorting processes accompanying the formation of secretory vesicles (*3*, *45*). However, the magnitude of the sterol flux through the secretory pathway has not been determined, and it is possible that it could be quite low in the absence of a "sphingolipid retainer" to prevent the loss of sterols from transport vesicles.

A Model for ER−PM Ergosterol Transport. The identical specific radioactivity of cellular and MβCD-extractable ergosterol at the end of the chase period (RSR ~ 1; Figures 2C and 3C), as well as the inability of *sec* mutants to block transport (Figure 3D), indicates that sterol transport between the ER and PM occurs by a nonvesicular pathway that leads to equilibration of sterol pools. Such a pathway would likely involve collision-mediated abstraction of sterol from the cytoplasmic leaflet of the donor compartment by either a soluble acceptor or an acceptor membrane. Because sterol flip-flop across liposomal membranes and biomembranes is rapid (*16*, *32*, *34*), sterols in the lumenal leaflet of donor and acceptor compartments also effectively become part of the transportable pool. Given this situation, how is it possible for the PM to maintain its high sterol concentration relative to the ER or with respect to other internal membranes?

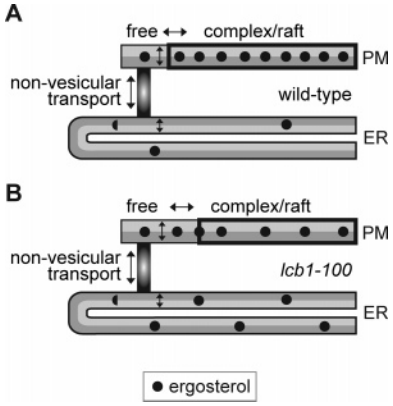

FIGURE 4: Model for transport of free sterols between the ER and PM. (A) Schematic illustrates ER−PM ergosterol transport based on the following: (a) ergosterol concentration in the PM is 10-fold higher than in the ER (*5*) (C. Simonot and A. K. Menon, unpublished); (b) ER membrane area in yeast is 2.5-fold greater than that of the PM (G. Zellnig, Karl-Franzens Universität Graz, personal communication); flip-flop of free sterols across both the ER and PM is rapid (*16*, *31*, *34*); (c) majority of PM ergosterol is associated with sphingolipids in the form of condensed complexes or rafts [this is reflected in the high fraction (~70%) of ergosterol in DIMs prepared from whole cells (the fraction would be expected to be higher in purified PM) and in the low extractability of ergosterol from wild-type cells by MβCD]; (d) pools of free and raft sterol in the PM are in equilibrium; (e) chemical activity of sterol in the ER [~concentration of free sterol (*11*)] is the same as it is in the PM; (f) free sterol in the PM is in equilibrium with the free sterol pool in the ER; equilibration is mediated by nonvesicular transport of free sterol between the two compartments. The illustration shows the PM and ER membranes drawn proportionately such that their length reflects their relative membrane area (PM ~ 1 area unit; ER ~ 2.5 area units). Ergosterol is depicted as ●; the number of ● in the PM (10 circles) and ER (2.5 circles) reflects the (relative) ergosterol content of the two organelles. Thus, the relative ergosterol concentration ([Σ sterol] = Σ sterol/area) in the PM and ER is 10 and 1, respectively. The circles are positioned in the middle of the bilayer to indicate the equivalence of the two membrane leaflets because of rapid flip-flop of free sterol. The figure shows that 90% of PM ergosterol is in rafts; all ER ergosterol is shown to be free although a small fraction could be raft-associated (*37*). The relative chemical activity of ergosterol ([free sterol]) is thus 1 in both the PM and ER. (B) Model shown in A is adapted for *lcb1−100* cells by decreasing the amount of complexed sterol by 2-fold in concert with the 2-fold lower level of sphingolipid in these cells. The model predicts that the total sterol in the PM in *lcb1−100* is lower than that in wild-type cells and that the amount of free sterol at the PM in *lcb1−100* is higher than that in wild-type cells. Both predictions are borne out by the data presented in Table 1.

One hypothesis, highlighted in recent speculations by McConnell et al. (*11*), is that the bulk of PM sterol is in the form of condensed complexes (rafts) and that the chemical activity or concentration of free sterol in the PM is identical to that in the ER. This proposal is compatible with nonvesicular transport of sterols between the ER and PM because only free sterol would be capable of being transported; sterols in condensed complexes have a significantly lower off rate from the membrane and would not be efficiently picked up by sterol acceptors. Figure 4A illustrates one variation of

Table 1: Properties of Wild-Type (RH1800) and *lcb1−100* (RH3809) Cells under Permissive (Room Temperature) and Restrictive Conditions (37 °C)

	room temperature		37 °C for 60 min	
	wild type	*lcb1−100*	wild type	*lcb1−100*
Erg/PL (nmol/nmol)[a,b]	0.547 ± 0.045	0.640 ± 0.053	0.476 ± 0.027	0.560 ± 0.023
Erg ester/PL (nmol/nmol)[b]	0.080 ± 0.025	0.110 ± 0.035	0.087 ± 0.006	0.100 ± 0.018
percent ergosterol in DIMs[c]	62.6 ± 5.0	46.7 ± 6.6	62.5 ± 15.1	48.3 ± 0.6
percent cellular ergosterol extracted by MβCD	ND[a]	ND[a]	0.36 ± 0.07	3.34 ± 0.63
sphingolipid (cpm/A_{600})[d]				
$M(IP)_2C$[a]	70.5 ± 8	55 ± 1	NA[a]	NA[a]
IPC + MIPC[a]	46 ± 6	11 ± 1	NA[a]	NA[a]

[a] Abbreviations: Erg, ergosterol; IPC, inositol-phosphoceramide; MIPC, mannose-inositol-phosphoceramide; $M(IP)_2C$, mannose(inositol phosphate)$_2$-ceramide; PL, phospholipid; ND, not determined; NA, not available. [b] Phospholipid determination was carried out by the method of Rouser et al. (*55*). [c] Bagnat et al. (*37*) reported similar results: sterol recovery in DIMs from wild-type and *lcb1−100* cells grown at room temperature was 59.4 ± 2.1 and 49.3 ± 7.3%, respectively. For cells incubated for 2 h at 37 °C, sterol recovery in DIMs was 56.7 ± 6.9 and 28.4 ± 8.2%, for wild-type and *lcb1−100*, respectively. [d] Data are reproduced from Hearn et al. (*48*). Cells were grown for at least 10 generations in the presence of [^{3}H]inositol and sphingolipids ($M(IP)_2C$, IPC, and MIPC), extracted, and quantitated. The level of complex sphingolipids is reduced ∼55% in *lcb1−100* cells relative to wild-type cells.

this idea using available data for the relative membrane area of the PM and ER in yeast (PM/ER area ∼ 1:2.5), the ergosterol concentration difference between the two organelles (10-fold), and the proportion of ergosterol in DIMs/rafts (>70%). The model incorporates the notion that the concentration of free sterol is the same in the PM and ER and indicates how it would be possible to have a pool of free ergosterol in the PM in equilibrium with a raft-associated pool of ergosterol in the PM as well as with a pool of free sterol in the ER. The model can be readily generalized to include other repositories of sterol in the cell, such as sterol esters that make up ∼15% of the sterol pool in yeast under our growth and pulse-chase conditions and that rapidly achieve the same SR as the total cellular sterol pool. Generalization of the model to include sterol pools in other internal membranes (such as vacuolar, endosomal, or mitochondrial membranes) would not affect its principle features, provided that a transport mechanism (carrier or contact site, for example) existed to facilitate intercompartment exchange of the free sterol pool.

Characterization of Sphingolipid-Deficient lcb1−100 Cells. To test the model presented in Figure 4A and to learn more about the mechanism by which sterols are transported to the PM, we investigated the consequences of altering the pool size of free sterol in the cell by assaying ergosterol transport in a yeast strain with a lower level of complex sphingolipids. A general consideration of transport between ER and PM pools of ergosterol[5] in a closed system at steady state suggests that equilibration should be reached slightly more rapidly when the pool size of free sterol is increased. However, if the velocity of sterol transport is already at its maximum level in wild-type cells, then the rate of equilibration will be slower on account of the greater pool of free sterol to be transported.

The *lcb1−100* ceramide synthesis mutant (*25*, *37*, *47*, *48*) was originally characterized as having a temperature-sensitive defect in serine palmitoyltransferase activity required for the first step of ceramide biosynthesis (*47*) but subsequently shown to have a 2-fold lower sphingolipid content compared to an isogenic wild-type strain even at the permissive temperature (*48*; data reproduced in Table 1). We hypothesized that the 2-fold lower sphingolipid level in *lcb1−100* would result in a proportionately larger cellular pool of free sterol compared to that in wild-type cells, potentially affecting the rate of equilibration of newly synthesized [^{3}H]-ergosterol in the MβCD-extractable sterol pool with the cellular pool.

Total ergosterol and ergosterol ester levels were essentially identical between *lcb1−100* and wild-type cells, regardless of whether the cells were grown at the permissive temperature or held at the restrictive temperature for 1 h (Table 1). However, the recovery of total cellular ergosterol in DIMs was lower in *lcb1−100* than in wild-type cells at both permissive and restrictive temperatures (Table 1). Also, the efficiency with which ergosterol could be extracted by MβCD treatment of *lcb1−100* cells under standard conditions was an order of magnitude higher compared with wild-type cells (Table 1). These observations are consistent with our prediction of a larger cellular pool of free sterol in *lcb1−100* cells versus their wild-type counterparts.

Figure 4B provides a model of the disposition of sterols in *lcb1−100*. The model is a modification of the model for wild-type cells presented in Figure 4A. It was generated by decreasing the number of complexed sterols in the PM 2-fold (to reflect the decrease in sphingolipid levels) while ensuring that the concentration of free sterols remained approximately the same in the PM and in the ER. The increased efficiency of MβCD-mediated ergosterol extraction in *lcb1−100* (Table 1) is qualitatively consistent with the increase in the amount of free sterol in the PM as depicted in the model.

The model (Figure 4B) predicts a ∼30% decrease in the total sterol content of the PM in *lcb1−100* compared to wild-type cells and an increase in sterol levels in the ER. To test this prediction, we used RenoCal gradients (*28*) to isolate PM fractions from crude membranes derived from *lcb1−100* and wild-type cells. We isolated PM from cells grown exclusively at the permissive temperature, as well as from cells that had been incubated for 1 h at the restrictive temperature (37 °C). Figure 5A shows that the relative sterol

[5] We assume that there are three pools of ergosterol in the system, a pool of free ergosterol in the ER and two pools, free and sphingolipid complexed, of ergosterol in the PM. The PM pools of ergosterol are proposed to be in rapid equilibrium with each other. The pools of free ergosterol in the ER and PM exchange through the cytoplasm via nonvesicular, bidirectional processes involving, for example, membrane contacts and/or lipid transfer proteins (see Figure 5). For a kinetic analysis of this problem, see ref *46*.

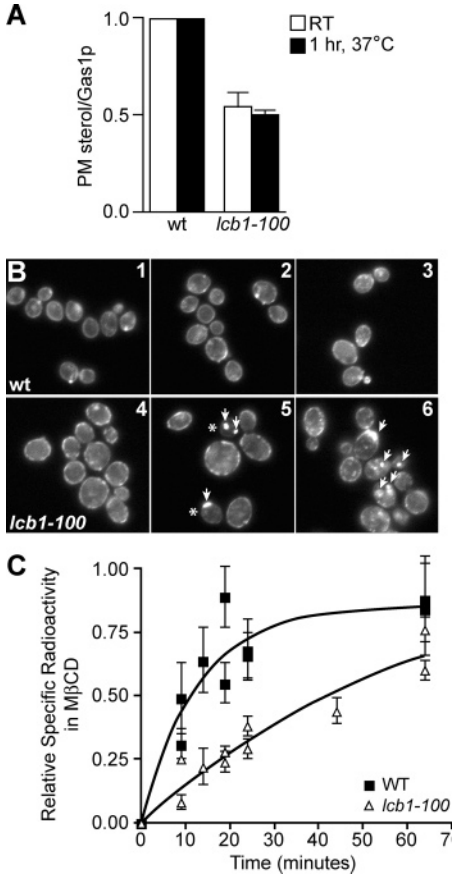

FIGURE 5: Subcellular sterol distribution and transport of newly synthesized ergosterol in *lcb1−100* cells. (A) Concentration of sterol in the PM of wild-type (wt) and *lcb1−100* cells. PM fractions were isolated on RenoCal gradients and characterized by lipid extraction and sterol determination by RP-HPLC, as well as quantitative immunoblotting using antibodies to Gas1p or Pma1p. The chart shows the sterol/Gas1p ratio for the PM of *lcb1−100* cells grown at room temperature (open bar) or held for 1 h at 37 °C (filled bar), relative to that of similarly grown wild-type cells (the data represent three independent experiments at each of the temperature conditions tested). The relative ratio using Pma1p instead of Gas1p was 0.54 ± 0.03 for *lcb1−100* PM (compared to 1 for wt PM). (B) Accumulation of intracellular sterol in *lcb1−100* mutant cells. (Panels 1−3) Filipin-stained wild-type (RH1800) cells, and (panels 4−6) filipin-stained *lcb1−100* (RH3809) cells. Cells were cultured in synthetic complete medium at 23 °C and then incubated at 37 °C for 0 h (panels 1 and 4), 1 h (panels 2 and 5), or 4 h (panels 3 and 6). Arrows indicate filipin fluorescence associated with spots within cells. At 23 °C, internal fluorescent spots were observed in 22.5% wild-type cells and 19.5% *lcb1−100*. After shifting to 37 °C for 1 h, internal spots were observed in 15.5% wild-type cells and in 41% *lcb1−100* cells. After 4 h at 37 °C, internal spots were observed in 19% wild-type cells and in 36.5% *lcb1−100* cells. For each strain and each of the incubation conditions tested, $n = 200$ cells counted. For PM staining, 11% of *lcb1−100* cells exhibited reduced filipin staining after 4 h at 37 °C, 6% of *lcb1−100* cells after 1 h at 37 °C, and 3% at 23 °C. After incubation for 4 h at 37 °C, only 2% of the wild-type cells exhibited reduced PM fluorescence. After 1 h at 37 °C, only 1% had reduced fluorescence, and at 23 °C just 1% wild-type cells had a clear reduction in PM filipin staining. For PM counting, $n = 100$ cells were counted for each strain and each incubation condition. Asterisks indicate examples of cells where PM filipin staining is significantly reduced or absent. The images shown represent equal exposures. Comparable results were obtained when cells were grown in synthetic or YPD rich medium (not shown). (C) Isotopic equilibration of newly synthesized erogosterol in the MβCD-extractable ergosterol pool with the cellular pool measured in *lcb1−100* cells as well as in an isogenic wild-type strain at the restrictive temperature. Experimental details are as described in the captions to Figures 2 and 3.

concentration [nmoles of ergosterol normalized to the PM marker Gas1p (Gas1p levels were determined by quantitative immunoblotting as described in the Experimental Procedures)] in the PM of *lcb1−100* cells is ∼45−50% lower than it is in wild-type cells under both permissive and restrictive growth conditions. Although consistent with the prediction of the model, the reduction is somewhat larger than expected (∼45−50% versus the predicted ∼30%); this could be due to the participation of other intracellular membranes, in addition to the ER, as repositories for sterol in *lcb1−100* cells (see below). The temperature independence of the effect is consistent with the fact that *lcb1−100* cells are sphingolipid-deficient even at the permissive temperature (*48*; Table 1). Because the total levels of ergosterol and ergosterol ester are essentially identical between wild-type and *lcb1−100* (Table 1), the decrease in PM sterol levels that we measured in *lcb1−100* indicates that the level of ER sterol and/or other pools of intracellular sterol in these cells is higher than that in wild-type cells.

As a further test of the model, we used filipin, a sterol-specific fluorescent probe (*49*), to investigate sterol distribution in whole cells. Wild-type and *lcb1−100* cells were incubated at 23 °C, shifted to 37 °C for 1 or 4 h, and then stained with filipin to examine cellular sterol localization by fluorescence microscopy. In wild-type cells at all temperatures (panels 1−3 of Figure 5B) and *lcb1−100* cells at 23 °C (panel 4 of Figure 5B), filipin/sterol fluorescence was primarily observed at the PM but was also observed in a minority (∼20%) of cells as small cytoplasmic spots. In contrast, *lcb1−100* cells incubated at 37 °C for 1 or 4 h exhibited a significant increase in internal filipin staining (panels 5 and 6 of Figure 5B). Although the percentage of affected *lcb1−100* cells (∼40%) was equivalent after 1 or 4 h at 37 °C, the intensity of the intracellular sterol staining was greater after the longer incubation at 37 °C. A subtle reduction in PM filipin/sterol fluorescence was also detected in *lcb1−100* cells after incubation for 1 or 4 h at 37 °C (cells indicated with an asterisk in panel 4 of Figure 5B).

The intracellular filipin/sterol fluorescence seen in *lcb1−100* cells incubated for 1 or 4 h at 37 °C (panels 5 and 6 of Figure 5B) does not correspond to a typical ER staining pattern (*30*). This might reflect a morphological change in peripheral ER induced by *lcb1−100* defects or represent sterol accumulation in a distinct subcellular compartment-(s). We speculate that, although ER sterol levels likely increase in response to the sphingolipid deficiency of *lcb1−100* cells as suggested by the model (parts A versus B in Figure 4), the change is not large enough to be rendered perceptible by filipin staining because there is a capacity limit to the extent to which ER sterol levels can increase (*8*). Under these conditions, the accumulated intracellular sterol is forced into distinct compartments that are evident by filipin fluorescence (compare panel 4 with panels 5 and 6 of Figure 5B). The exact site of this intracellular accumulation bears investigation. Regardless, it is clear from our data that the intracellular accumulation of sterols in *lcb1−100* cells occurs at the expense of the PM sterol pool.

ER−PM Ergosterol Transport in lcb1−100 Cells. Assay of [^{3}H]ergosterol transport to the PM showed that the rate of equilibration of newly synthesized [^{3}H]ergosterol in the MβCD-extractable sterol pool with the cellular pool was ∼5-fold slower in *lcb1−100* cells compared with an isogenic

wild type at both permissive (not shown) and restrictive temperatures (Figure 5C). Because the *lcb1−100* cells have a greater cellular pool of free sterol compared to the wild-type cells, this suggests that the proposed nonvesicular transport mechanism is saturated under wild-type conditions.

Concluding Discussion. We have presented a simple model (Figure 4A) to explain sterol transport between the ER, the intracellular site of sterol biosynthesis, and the PM, the largest repository of sterol in the cell. The premise of the model is that sterol pools in the two membranes are at equilibrium and that it is the pool of free sterol in each compartment that is able to exchange bidirectionally through the cytoplasm. The model can be generalized to accommodate transport between the PM and other intracellular membranes; these membranes, like the ER, would have a characteristically low sterol concentration in wild-type cells. Our experiments with filipin staining suggest that, when sphingolipid levels are disturbed and the sterol-retaining ability of the PM is decreased, sterol is redistributed to intracellular structures. These structures, especially evident in *lcb1−100* cells that are stressed by incubation at the restrictive temperature, may be associated with the ER or correspond to an entirely separate compartment that is nevertheless connected to and part of the intracellular sterol equilibration pathway.

Intercompartmental equilibration of sterol pools could potentially encompass all cellular membranes if it involved a soluble carrier with no particular affinity for a particular membrane system. However, the recent discovery of CERT (*50*), a START-domain-containing lipid-transfer protein capable of ferrying ER-synthesized ceramide to the site of sphingomyelin synthesis in the Golgi, suggests that equilibration can be restricted to a specific pair of participating membranes. CERT has ER- and Golgi-binding sequences that would allow it to interact alternately with these compartments or potentially to bridge the two organelles at points of proximity. A similar molecular device could be involved in trafficking sterol between the ER (or other intracellular membrane) and PM. EM tomography indicates that there are ∼1000 ER−PM contact sites per yeast cell, defined by a gap of ∼30 nm (*51*, *52*). Recent work has identified yeast proteins that, like CERT, contain binding motifs that would allow them to engage two organelles, the ER and PM or the ER and vacuole (*30*, *53*, *54*). Such proteins may act to ensure that the contact site gap between the membrane pair is sufficiently small that collisional exchanges of sterol occur efficiently, or they may act as carriers themselves, appropriately situated at points of membrane contact. Their function may possibly be regulated by phosphorylation (the protein carrier itself could be phosphorylated, or it may require the presence of phosphorylated lipids such as the phosphorylated phosphoinositides to provide membrane-binding/docking sites), accounting for the ATP dependence of transport. Evaluating the relative role of lipid carriers, molecular bridges between organelles and membrane contact sites in ER−PM sterol transport, will be a challenge for future work.

ACKNOWLEDGMENT

We thank Bob Dickson for insight into the phenotype of *lcb1−100* cells, Gerrit van Meer for a critical contribution in interpreting the *lcb1−100* data, Tim Levine, Fred Maxfield, and W. W. Cleland for helpful discussions, Charles Barlowe and Howard Riezman for strains, Betty Craig, Patty Kane, Tom Rapoport, and Will Prinz for antibodies, Laura van der Ploeg for preparation of the figures, and George Harvey Bone, Bob Dylan, Axel Heyst, and Alec Leamas (assistant librarian) for stimulation.

REFERENCES

1. Liscum, L., and Munn, N. J. (1999) Intracellular cholesterol transport, *Biochim. Biophys. Acta 1438*, 19−37.
2. Maxfield, F. M., and Wüstner, D. (2002) Intracellular cholesterol transport, *J. Clin. Invest. 110*, 891−898.
3. Sprong, H., van der Sluijs, P., and van Meer, G. (2001) How proteins move lipids and lipids move proteins, *Nat. Rev. Mol. Cell Biol. 2*, 504−513.
4. Orci, L., Montesano, R., Meda, P., Malaisse-Lagae, F., Brown, D., Perrelet, A., and Vassalli, P. (1981) Heterogeneous distribution of filipin-cholesterol complexes across the cisternae of the Golgi apparatus, *Proc. Natl. Acad. Sci. U.S.A. 78*, 293−297.
5. Zinser, E., Sperka-Gottlieb, C. D. M., Fasch, E.-V., Kohlwein, S. D., Paltauf, F., and Daum, G. (1991) Phospholipid synthesis and lipid composition of subcellular membranes in the unicellular eukaryote *Saccharomyces cerevisiae*, *J. Bacteriol. 173*, 2026−2034.
6. Schneiter, R., Brügger, B., Sandhoff, R., Zellnig, G., Leber, A., Lampl, M., Athenstaedt, K., Hrastnik, C., Eder, S., Daum, G., Paltauf, F., Wieland, F. T., and Kohlwein, S. D. (1999) Electrospray ionization tandem mass spectrometry (ESI−MS/MS) analysis of the lipid molecular species composition of yeast subcellular membranes reveals acyl chain-based sorting/remodeling of distinct molecular species en route to the plasma membrane, *J. Cell Biol. 146*, 741−754.
7. Yeagle, P. L. (1993) *The Membranes of Cells*, 2nd ed., Academic Press, New York.
8. Nilsson, I., Ohvo-Rekilä, H., Slotte, J. P., Johnson, A. E., and von Heijne, G. (2001) Inhibition of protein translocation across the endoplasmic reticulum membrane by sterols, *J. Biol. Chem. 276*, 41748−41754.
9. Simons, K., and Ikonen, E. (2000) How cells handle cholesterol, *Science 290*, 1721−1726.
10. Brown, D. A., and London, E. (1998) Functions of lipid rafts in biological membranes, *Annu. Rev. Cell Dev. Biol. 14*, 111−136.
11. McConnell, H. M., and Vrljic, M. (2003) Liquid−liquid immiscibility in membranes, *Annu. Rev. Biophys. Biomol. Struct. 32*, 469−492.
12. Edidin, M. (2003) The state of lipid rafts: From model membranes to cells, *Annu. Rev. Biophys. Biomol. Struct. 32*, 257−283.
13. Mukherjee, S., and Maxfield, F. R. (2004) Membrane domains, *Annu. Rev. Cell Dev. Biol. 20*, 839−866.
14. Simons, K., and Toomre, D. (2000) Lipid rafts and signal transduction, *Nat. Rev. Mol. Cell Biol. 1*, 31−39.
15. Ohvo-Rekila, H., Ramstedt, B., Leppimaki, P., and Slotte, J. P. (2002) Cholesterol interactions with phospholipids in membranes, *Prog. Lipid Res. 41*, 66−97.
16. Leventis, R., and Silvius, J. R. (2001) Use of cyclodextrins to monitor transbilayer movement and differential lipid affinities of cholesterol, *Biophys. J. 81*, 2257−2267.
17. Frolov, A., Woodford, J. K., Murphy, E. J., Billheimer, J. T., and Schroeder, F. (1996) Spontaneous and protein-mediated sterol transfer between intracellular membranes, *J. Biol. Chem. 271*, 16075−16083.
18. Lange, Y., and Matthies, H. J. G. (1984) Transfer of cholesterol from its site of synthesis to the plasma membrane, *J. Biol. Chem. 259*, 14624−14630.
19. Kaplan, M. R., and Simoni, R. D. (1985) Transport of cholesterol from the endoplasmic reticulum to the plasma membrane, *J. Cell Biol. 101*, 446−453.
20. Urbani, L., and Simoni, R. D. (1990) Cholesterol and vesicular stomatitis virus G protein take separate routes from the endoplasmic reticulum to the plasma membrane, *J. Biol. Chem. 265*, 1919−1923.
21. Heino, S., Lusa, S., Somerharju, P., Ehnholm, C., Olkkonen, V. M., and Ikonen, E. (2000) Dissecting the role of the golgi complex and lipid rafts in biosynthetic transport of cholesterol to the cell surface, *Proc. Natl. Acad. Sci. U.S.A. 97*, 8375−8380.

22. Sturley, S. L. (2000) Conservation of eukaryotic sterol homeostasis: New insights from studies in budding yeast, *Biochim. Biophys. Acta 1529*, 155−163.
23. Novick, P., Field, C., and Schekman, R. (1980) Identification of 23 complementation groups required for post-translational events in the yeast secretory pathway, *Cell 21*, 205−215.
24. Kaiser, C. A., and Schekman, R. (1990) Distinct sets of SEC genes govern transport vesicle formation and fusion early in the secretory pathway, *Cell 61*, 723−733.
25. Zanolari, B., Friant, S., Funato, K., Sütterlin, C., Stevenson, B. J., and Riezman, H. (2000) Sphingoid base synthesis requirement for endocytosis in *Saccharomyces cerevisiae*, *EMBO J. 19*, 2824−2833.
26. Deere, D., Shen, J., Vesey, G., Bell, P., Bissinger, P., and Veal D. (1998) Flow cytometry and cell sorting for yeast viability assessment and cell selection, *Yeast 14*, 147−160.
27. Rodriguez, R. J., and Parks, L. W. (1985) High performance liquid chromatography of sterols: Yeast sterols, *Methods Enzymol. 111*, 37−51.
28. Chang, A. (2002) Plasma membrane biogenesis, *Methods Enzymol. 351*, 339−350.
29. Li, Y., and Prinz, W. A. (2004) ATP-binding cassette (ABC) transporters mediate nonvesicular, raft-modulated sterol movement from the plasma membrane to the endoplasmic reticulum, *J. Biol. Chem. 279*, 45226−45234.
30. Beh, C. T., and Rine, J. (2004) A role for yeast oxysterol-binding protein homologs in endocytosis and in the maintenance of intracellular sterol−lipid distribution, *J. Cell Sci. 117*, 2983−2996.
31. Xu, X., Bittman, R., Duportail, G., Heissler, D., Vilcheze, C., and London, E. (2001) Effect of the structure of natural sterols and sphingolipids on the formation of ordered sphingolipid/sterol domains (rafts). Comparison of cholesterol to plant, fungal, and disease-associated sterols and comparison of sphingomyelin, cerebrosides, and ceramide, *J. Biol. Chem. 276*, 33540−33546.
32. Steck, T. L., Ye, J., and Lange, Y. (2002) Probing red cell membrane cholesterol movement with cyclodextrin, *Biophys. J. 83*, 2118−2125.
33. Yancey, P. G., Rodrigueza, W. V., Kilsdonk, E. P. C., Stoudt, G. W., Johnson, W. J., Phillips, M. C., and Rothblat, G. H. (1996) Cellular cholesterol efflux mediated by cyclodextrins. Demonstration of kinetic pools and mechanism of efflux, *J. Biol. Chem. 271*, 16026−16034.
34. John, K., Kubelt, J., Müller, P., Wüstner, D., and Herrmann, A. (2002) Rapid transbilayer movement of the fluorescent sterol dehydroergosterol in lipid membranes, *Biophys. J. 83*, 1525−1534.
35. Greenberg, M. L., and Axelrod, D. (1993) Anomalously slow mobility of fluorescent lipid probes in the plasma membrane of the yeast *Saccharomyces cerevisiae*, *J. Membr. Biol. 131*, 115−127.
36. Valdez-Taubas, J., and Pelham, H. R. B. (2003) Slow diffusion of proteins in the yeast plasma membrane allows polarity to be maintained by endocytic cycling, *Curr. Biol. 13*, 1636−1640.
37. Bagnat, M., Keränen, S., Shevchenko, A., Shevchenko, A., and Simons, K. (2000) Lipid rafts function in biosynthetic delivery of proteins to the cell surface in yeast, *Proc. Natl. Acad. Sci. U.S.A. 97*, 3254−3259.
38. Wilson, D. W., Wilcox, C. A., Flynn, G. C., Chen, E., Kuang, W.-J., Henzel, W. J., Block, M. R., Ulrich, A., and Rothman, J. E. (1989) A fusion protein required for vesicle-mediated transport in both mammalian cells and yeast, *Nature 339*, 355−359.
39. Graham, T. R., and Emr, S. D. (1991) Compartmental organization of Golgi-specific protein modification and vacuolar protein sorting events defined in a yeast sec18 (NSF) mutant, *J. Cell Biol. 114*, 207−218.
40. Levine, T. P., Wiggins, C. A. R., and Munro, S. (2000) Inositol phosphorylceramide synthase is located in the Golgi apparatus of *Saccharomyces cerevisiae*, *Mol. Biol. Cell 11*, 2267−2281.
41. Funato, K., and Riezman, H. (2001) Vesicular and nonvesicular transport of ceramide from the ER to the Golgi apparatus in yeast, *J. Cell Biol. 155*, 949−959.
42. Puoti, A., Desponds, C., and Conzelmann, A. (1991) Biosynthesis of mannosylinositolphosphoceramide in *Saccharomyces cerevisiae* is dependent on genes controlling the flow of secretory vesicles from the endoplasmic reticulum to the Golgi, *J. Cell Biol. 113*, 515−525.
43. Barlowe, C., and Schekman, R. (1993) SEC12 encodes a guanine nucleotide exchange factor essential for transport vesicle formation from the ER, *Nature 365*, 347−349.
44. Grote, E., Carr, C. M., and Novick, P. J. (2000) Ordering the final events in yeast exocytosis, *J. Cell Biol. 151*, 439−451.
45. Brügger, B., Sandhoff, R., Wegehingel, S., Gorgas, K., Malsam, J., Helms, J. B., Lehmann, W.-D., Nickel, W., and Wieland, F. T. (2000) Evidence for segregation of sphingomyelin and cholesterol during formation of COPI-coated vesicles, *J. Cell Biol. 151*, 507−517.
46. Shipley, R. A., and Clark, R. E. (1972) *Tracer Methods for in Vivo Kinetics: Theory and Applications*, Chapter 8, Academic Press, New York.
47. Sütterlin, C., Doering, T. L., Schimmöller, F., Schroder, S., and Riezman, H. (1997) Specific requirements for the ER to Golgi transport of GPI-anchored proteins in yeast, *J. Cell Sci. 110*, 2703−2714.
48. Hearn, J. D., Lester, R. L., and Dickson, R. C. (2003) The uracil transporter Fur4p associates with lipid rafts, *J. Biol. Chem. 278*, 3679−3686.
49. Severs, N. J. (1997) Cholesterol cytochemistry in cell biology and disease, *Subcell. Biochem. 28*, 477−505.
50. Hanada, K., Kumagai, K,. Yasuda, S., Miura, Y., Kawano, M., Fukasawa, M., and Nishijima, M. (2003) Molecular machinery for non-vesicular trafficking of ceramide, *Nature 426*, 803−809.
51. Pichler, H., Gaigg, B., Hrastnik, C., Achleitner, G., Kohlwein, S. D., Zellnig, G., Perktold, A., and Daum, G. (2001) A subfraction of the yeast endoplasmic reticulum associates with the plasma membrane and has a high capacity to synthesize lipids, *Eur. J. Biochem. 268*, 2351−2361.
52. Levine, T. (2004) Short-range intracellular trafficking of small molecules across endoplasmic reticulum junctions, *Trends Cell Biol. 14*, 483−490.
53. Levine, T. P., and Munro, S. (2001) Dual targeting of Osh1p, a yeast homologue of oxysterol-binding protein, to both the Golgi and the nucleus-vacuole junction, *Mol. Biol. Cell 12*, 1633−1644.
54. Loewen, C. J. R., Roy, A., and Levine, T. P. (2003) A conserved ER targeting motif in three families of lipid binding proteins and in Opi1p binds VAP, *EMBO J. 22*, 2025−2035.
55. Rouser, G., Fleischer, S., and Yamamoto, A. (1970) Two-dimensional thin layer chromatographic separation of polar lipids and determination of phospholipids by phosphorus analysis of spots, *Lipids 5*, 494−496.

BI048296Z